# SUPPLEMENTAL INFORMATION

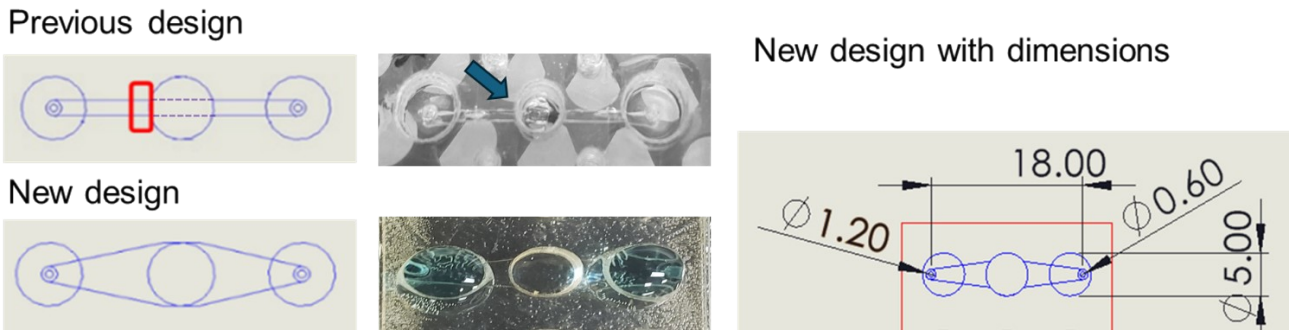


**Figure S1. Comparison of the previous design and the new design of the RWM model.** Left: the bubble-generated region was marked in red, and the arrow indicated a bubble formation (upper left); the image of the new design without bubble formation (lower left). Right: the dimensions of the singlet new device in mm.

PET membranes were either treated with oxygen plasma for 2 minutes or left untreated. And then those membranes were plated in individual wells of 6-well tissue culture plates. SAEC and RPTEC were seeded on top of the membranes. After 48 h, the membranes were transferred to new 6-well tissue culture plates, and Live & dead assay was performed. All of the three types of cells cultured on the PET membranes (**Figure S2A**) have good cell viability (>95%). There was no significant difference in cell survival rate between the plasma-treated membrane group and the untreated group, which indicated that the natural hydrophilic PET membrane can support the growth of all three types of epithelial cells. The only difference was the cell density of RPTEC in the untreated group was slightly less than the group treated with plasma and cell morphology was more stretched in the plasma-treated group compared to the untreated group.

To optimize the design of the microfluidic devices, we tested whether the presence of collagen will increase the RPTEC cell density/number in microfluidic devices. We prepared 150 µg/mL collagen I solution, Rat Tail (Corning, NY) in 0.01M HCl solution, and allowed collagen solution in devices to settle at room temperature for 1 hour. After that, excess collagen was discarded by aspirating liquid from channels, and the channels were washed with tissue-culture grade sterilized water, then 1 X PBS, by pipetting directly into the channel openings before seeding cells. **Figure S2B** demonstrates that the presence of collagen increases the RPTEC cell density on the membrane.

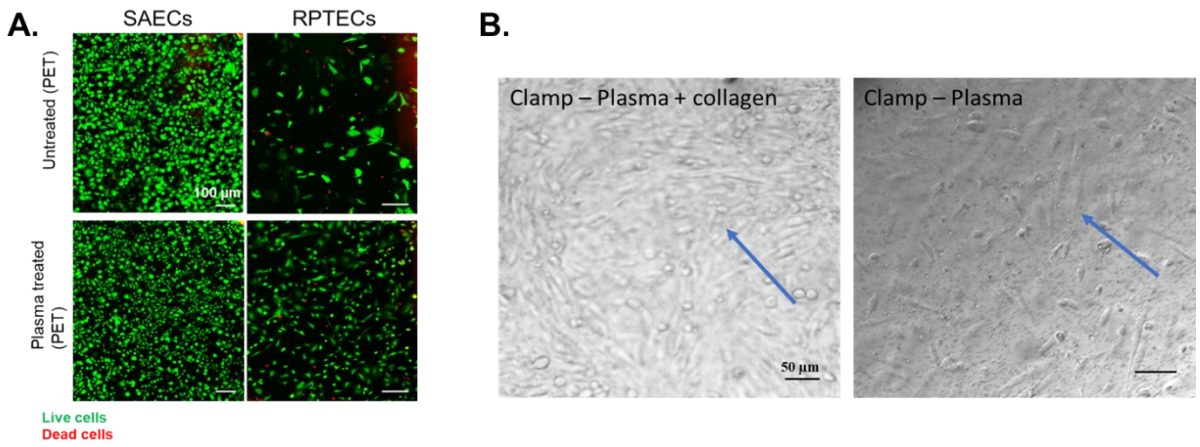


**Figure S2. Optimization of cell seeding in PET membrane.** A. 2 cell types seeded on PET membrane with and without plasma treatment. B. RPTEC cell seeding on PET membrane with and without collagen coating.

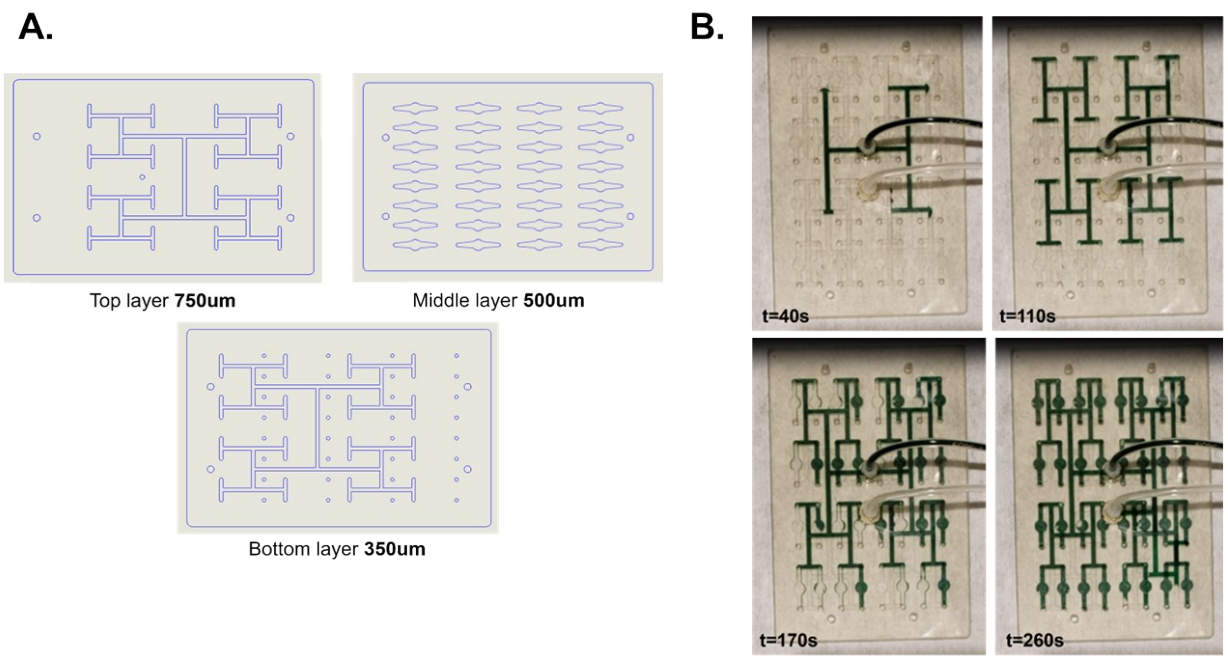


**Figure S3. Design of fluidic distribution plate.** A. Individual layer thicknesses of the fluid distribution plate. These optimum thickness values were found after an extensive number of fluid distribution experiments. We observed that the optimum condition is achieved if the fluidic resistances are increasing from layer to layer so that the least resistance should be the first layer and the highest hydraulic resistance should correspond to the last layer that connects the outlets. In this way, the liquid fills each layer before passing to the next higher resistance layer. B. Snapshots from the flow experiment showing all 32 devices are filled successfully without leaving any empty device.

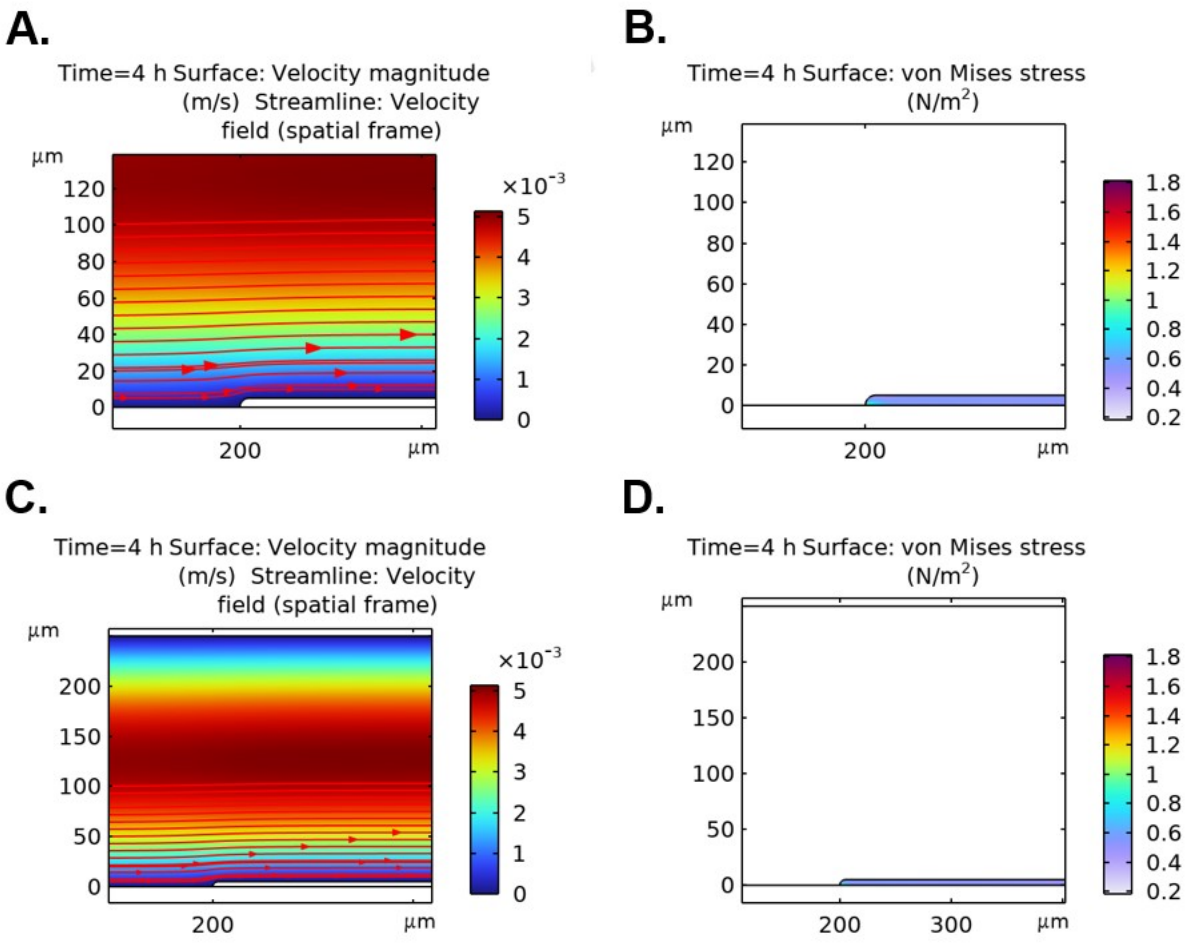


**Figure S4. COMSOL Multiphysics modeling of flow speed and cell shear stress.** A. The 2D COMSOL model revealed the flow speed distribution above the modeled hair cells. B. Demonstration of the flow's impact on the shear force in the 10 µm thick layer of cells. Our results showed that the induced von Mises stress is below 0.3 N/m² at the maximum flow speed. C. The overview of the flow velocity distribution across the entire channel. D. The overview of the von Mises stress distribution across the entire channel.

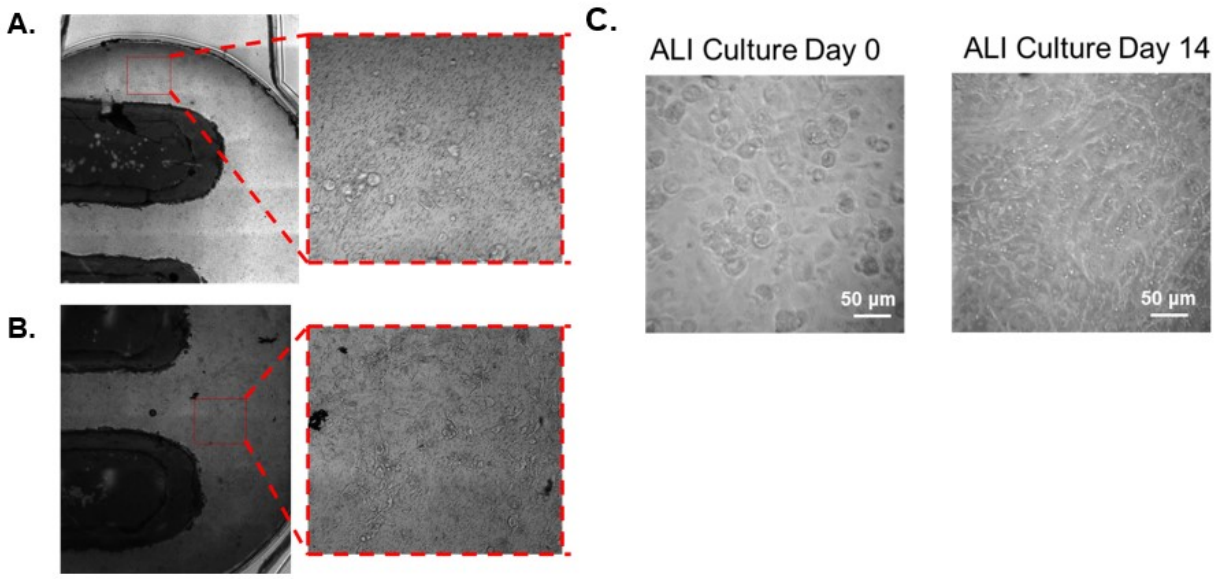


**Figure S5. TEER device cell seeding.** Brightfield images of SAEC seeded on porous PET membrane within the TEER-embedded microfluidic chip on (A) D1 and (B) D8. SAEC adhere and proliferate in the presence of gold electrodes (oblong black geometry) within the cell culture space. C. Phase-contrast images of the cell morphology before and after a 14-day ALI culture.

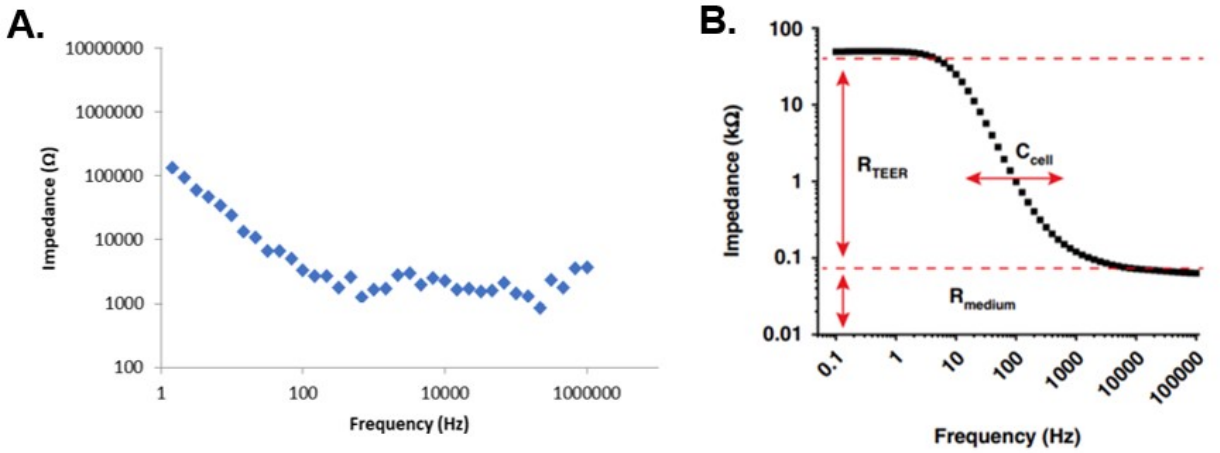


**Figure S6. TEER sensor performance.** A. Representative EIS spectra from devices on D8. B. Bode curve for TEER detection by Electrochemical Impedance Spectroscopy.

**Protein sensor development**

We followed the sensor functionalization and testing protocol described by Xu et al[1], using the same commercial GFET sensor (Graphenea GFET S20) for all our testing. The entire GFET S20 chip was immersed in methanol for 30 minutes for cleaning, then retrieved and dried with compressed air. 1-pyrenebutanoic acid succinimidyl ester (PBASE) was dissolved in N-Dimethylformamide (DMF) to a final concentration of 10 mM. A 30 µL drop of the 10 mM PBASE solution was added to the center area of the GFET S20 chip and incubated for 2 hours at room temperature in the dark. The PBASE was then removed by blotting with a rolled-up tip of a Kimwipe, and the center area of the GFET S20 chip was washed with DMF. GFET chip was functionalized with a recognition element (aptamer), exposing analytes to the sensor. We introduced an incubation step, where the aptamer was introduced to the analyte mixture before sensor exposure. If the aptamer successfully binds the analyte, we anticipate conformation change that impacts interaction with the GFET. To design and develop a TNF-α sensor, the analyte was mixed for at least one hour with the published aptamer selected for recognition. These samples are first tested by are then dropped on fresh GFET sensors for comparison. The concentration calibration curve was made by standard samples. We used two potentiates for protein sensing. BioLogic was used to vary the gate voltage (between 0.5 – 0.9V) while the corresponding current response of the GFET sensors were measured using the Palmsens 4. The reference electrode and the drain electrode were connected to the Biologic, and the gate electrode were connected to the Palmsens 4, where a constant voltage of 0.1V was applied. The time stamps from the voltage sweep and the current recording were aligned to produce the current vs voltage graph of the Dirac shift due to protein binding.

Polydimethylsiloxane (PDMS) was used to facilitate fluid flow and analyte detection via GFET biosensor. Briefly, microfluidic channels were formed in PDMS using the template as a mold; base and curing agent (Sylgard 184) were pre-mixed in a 1:10 ratio, then cured at 80°C for at least 2 h per manufacturer instructions. The PDMS channels were cut to the appropriate size, treated with oxygen plasma to expose silanol groups, and then immediately adhered to chips. To promote adherence between the PDMS and silicon regions of the GFET chip, GFET chips were exposed to oxygen plasma from a corona plasma wand for ~2 seconds at a working distance of an inch. Exposure was limited to 2 seconds to prevent destruction of the graphene elements within the GFET chip.

**TNF-α sensing testing**

For GFET sensor development, we use proinflammatory cytokine TNF-α as an example to demonstrate the integrated MPS platform (**Figure S7A**). The aptamer sequencing was 5'-GCGCCACTACAGGGGAGCTGCCATTCGAATAGGTGGGCCGC-3' and reference aptamer sequencing was 5'-TGAAGAGGCATGCCGACTGATGTCGATCTCGCATCCGTAACTGACGTACGA-3' [2]. We demonstrate proof of feasibility using TNF-α (0.7 µg/mL). The resulting data (**Figure S7B**) indicates a sharp drop in current when blank PBS solution is dropped onto a dry sensor. Upon addition of the premixed Test and Control samples, unattached aptamer chains quickly adhere to the graphene while available pyrene anchors more slowly become established. More pyrene on the surface leads to higher conductivity across the graphene.

We envision a measurement sequence that begins with a background buffer (sans analyte) to baseline the sensor in the presence of any ionic species and other possible interferents. The signal will then be differential measurements from this baseline with an additional sample introduced containing possible aptamer-analyte pairs, as seen with TNF-α. Negative binding results indicated by a decreased current form aptamer adsorption alone can be rinsed away according to our testing.

In our experiments, the following reagents were applied to the same chip during continuous measurements: 1x PBS buffer, 70 ng/ml TNF-α, 700 ng/ml TNF-α, and 7 µg/ml TNF-α samples in PBS, followed by a 1-hour incubation and washing with 1x PBS (**Figure S7C**). While the 70 ng/ml TNF-α sample did not result in a substantial increase in the measurements (**Figure S7C**, green frame), the 700 ng/ml TNF-α sample showed a clear increase in conductivity compared to the control samples (**Figure S7B**). A similar increase in GFET conductivity was observed when the more concentrated 7 µg/ml TNF-α sample was added to the chip (**Figure S7D**).

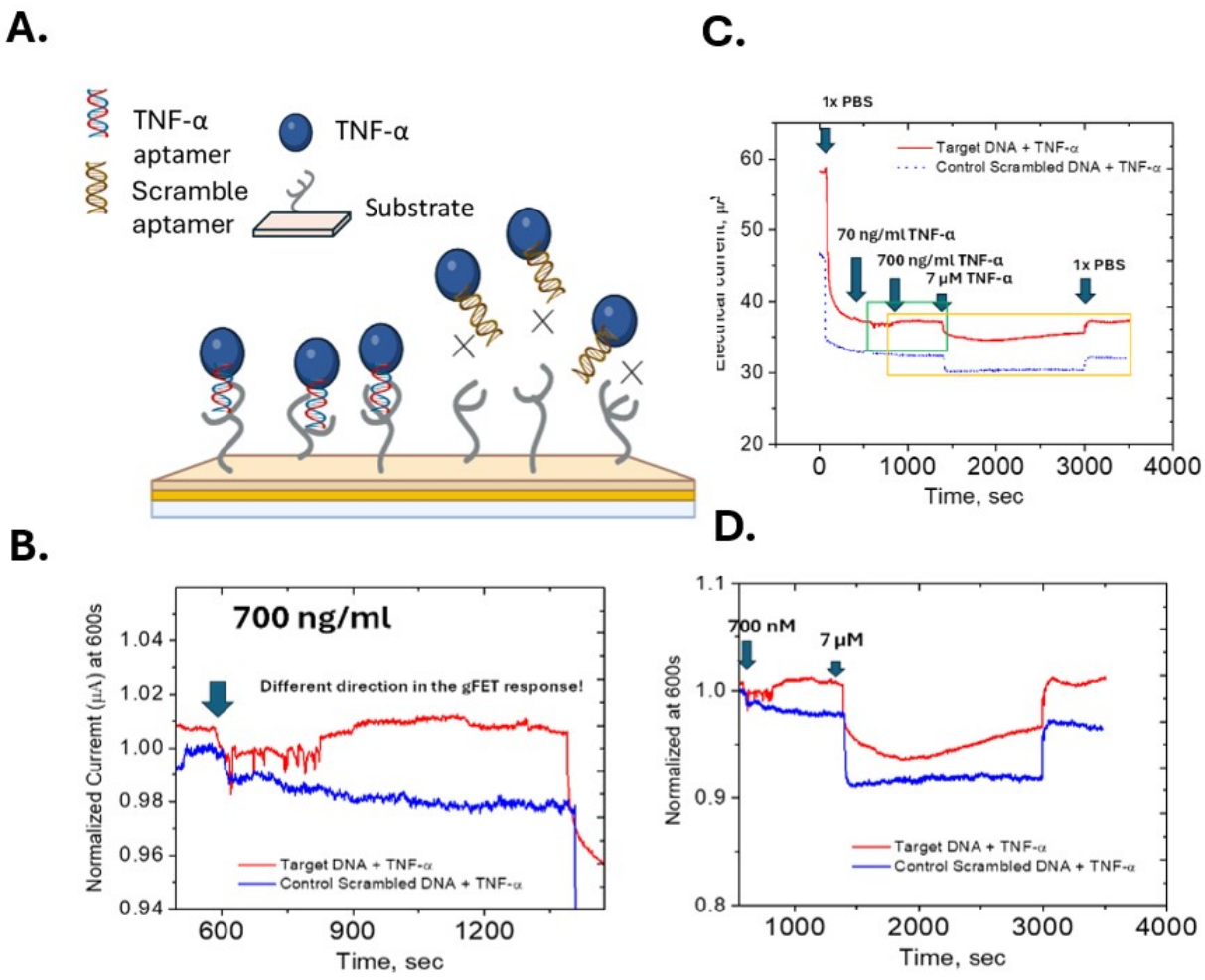

**Figure S7. TNF-α Sensing with GFET.** A: schematic of a Graphenea GFET with target and control DNA aptamers**;** B: the image demonstrates the restoration of conductivity upon the application of target DNA aptamers to TNF-α; C: the following samples were applied to a typical GFET device: 1x PBS buffer, 70 ng/ml TNF-α, 700 ng/ml TNF-α, and 7 μg/ml TNF-α in PBS, followed by a 1-hour incubation and washing with 1x PBS; D: a similar trend was observed when 10x more concentrated samples were applied. The increase in conductivity after applying 1x PBS buffer remained for the target sample, indicating a sustained rise in GFET conductivity (i.e., a decrease in resistance).

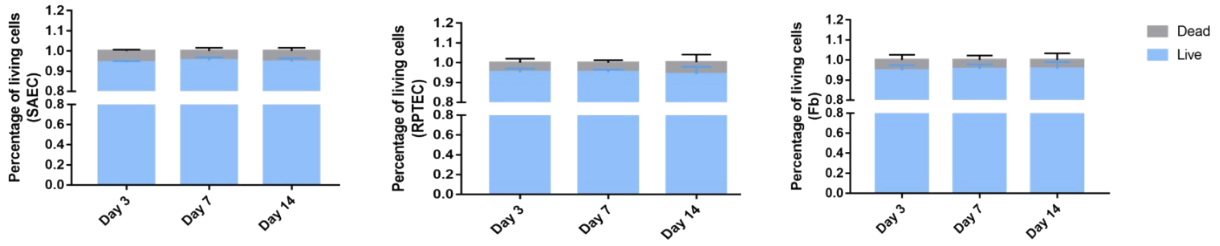


**Figure S8. Quantitative analysis of SAEC, RPTEC and HDF cell viability in coculture from Day 3 to Day 14.**

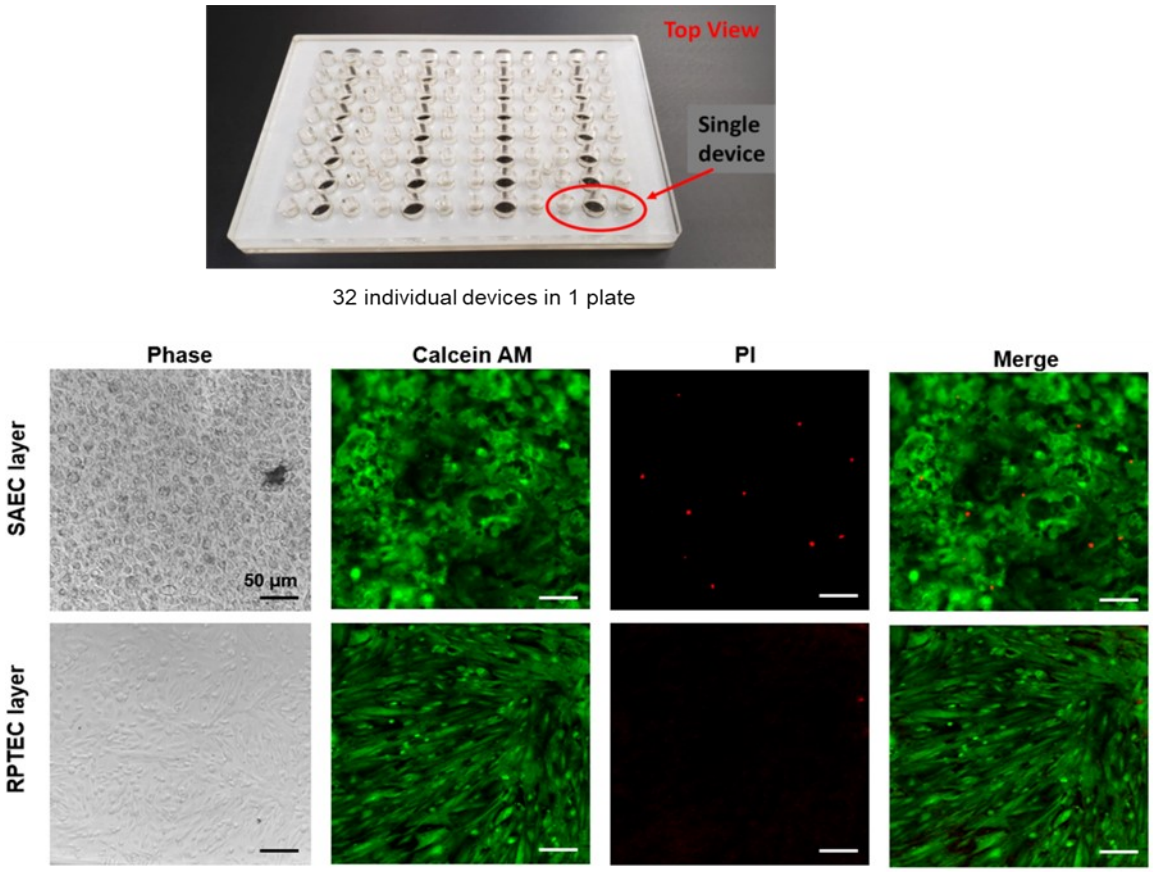


**Figure S9. Multiplex device for RWM model.** (Upper) image of the multiplex microfluidic device -top view; (lower) Live and dead staining/ phase contrast images of cells (SAEC and RPTEC) in RWM device after 14 days of ALI culture.

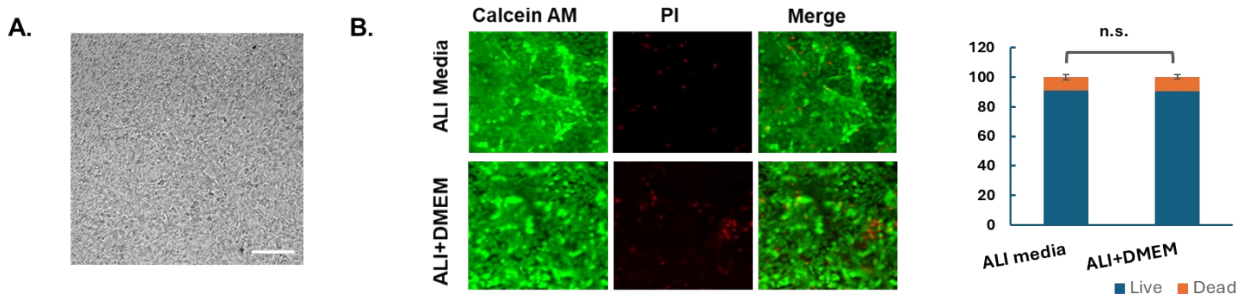


**Figure S10. Characterization of HEI-OC1 cell seeding and RWM-hair cell coculture.** A. HEI-OC1 cell morphology at 48 hours for 10,000 cells/device**.** B. (left) Fluorescence images of SAECs seeded on the upper well of the microfluidic device in co-culture as an example. Calcein AM (green)/PI (red) staining was performed 48 hours after cell growing in different media; (right) normalized RWM cell viability (3-cell types).

We constructed our new round window membrane. All the experimental steps were the same except for replacing the RPTEC cells with MEECs. We characterize the co-cultures by monitoring the formation of tight junctions for SAEC and MEEC (ZO-1). We observed SAEC ZO-1 expression on day 14 in the ALI culture indicating the formation of tight junctions (**Figure S11A**). SAEC also expressed a high level of mucous cell marker (MUC5AC) and goblet cell marker (beta-tubulin IV). Vimentin immunostaining was also performed to monitor the functionality of the HDF cells in the hydrogel during 14-day co-culturing. Also, MEEC is positive for the squamous epithelial cell marker (CK14) and tight junction marker ZO-1.

We have completed 14 days of TEER measurement for the RWM modes (**Figure S11B**). The RWM model exhibited similar TEER values on day 14 compared to the old RWM design. The TEER value was recorded ~320Ω.cm$^2$ on day 14 for the new RWM. However, on Day 28, we noticed a graduate degeneration of the MEEC monolayer formation (**Figure S11C**).

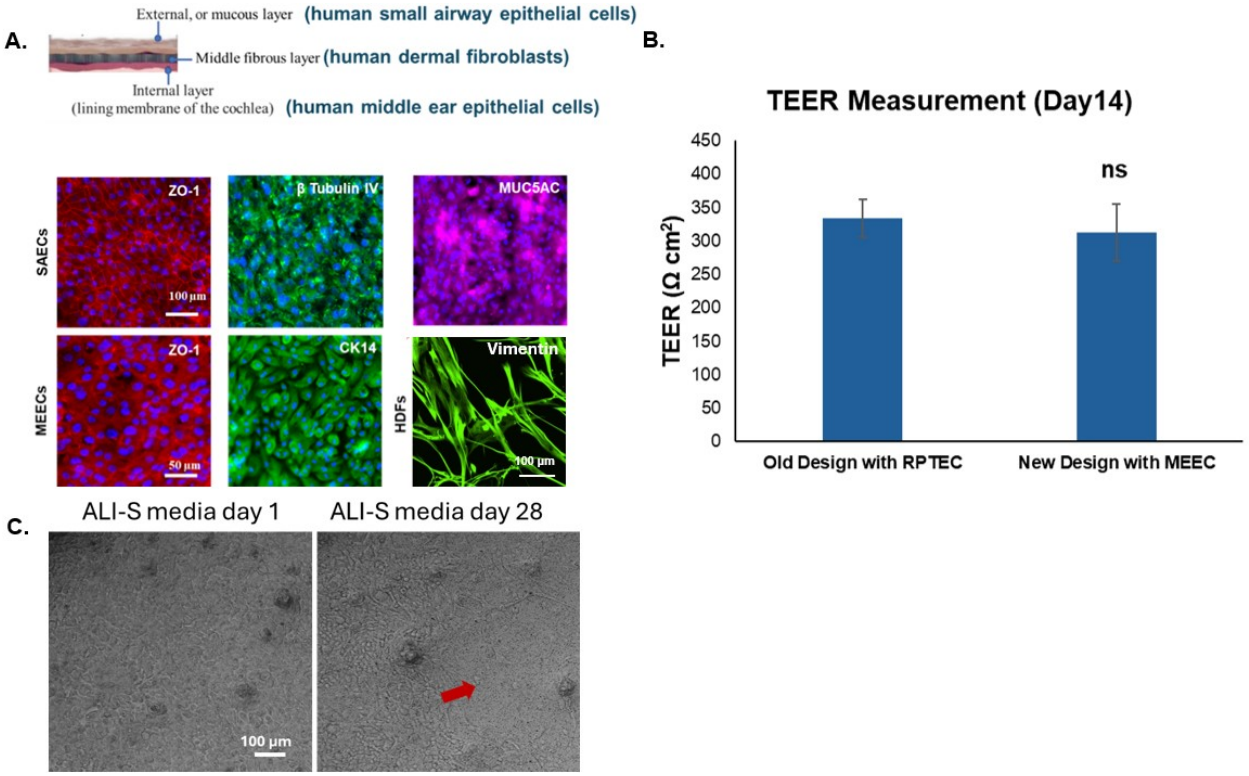


**Figure S11. New RWM model.** A. The layout of the new RWM and IF staining of relevant biomarkers. B. TEER development in the three-layered culture of the new RWM model in the engineered tissue constructs for 14 days. C. MEEC monolayer started to deform after long-term culture with ALI media (>28 days), red arrow – no cell region.

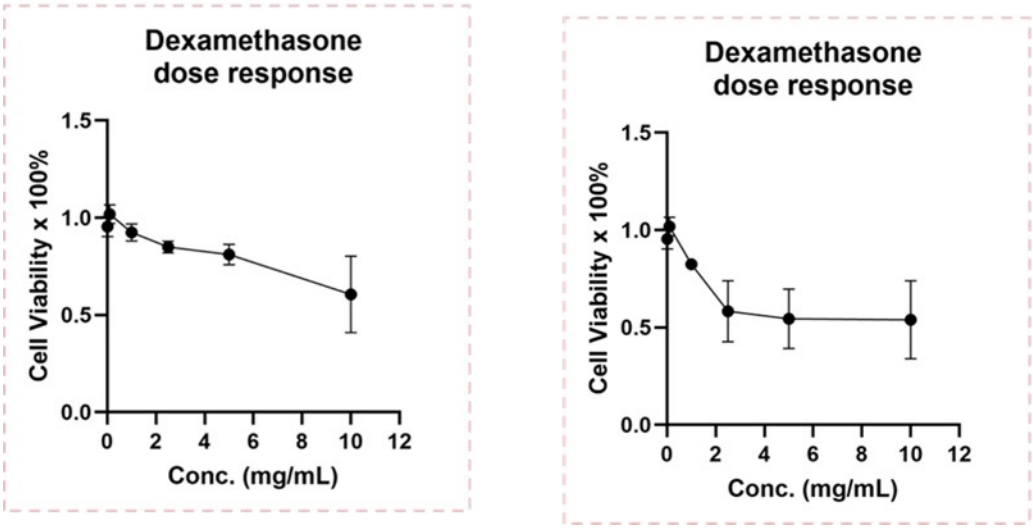


**Figure S12. Drug dose-dependent curve for dexamethasone using the new RWM model, for 48h, with and without the RWM. Left: normalized cell viability of RWM+HEI-OC1 cells; right: cell viability of HEI-OC1 cells. Compared to the old design using RPTEC, there are no significant differences in cell response in the presence of dexamethasone (compared to Figure 5C).**

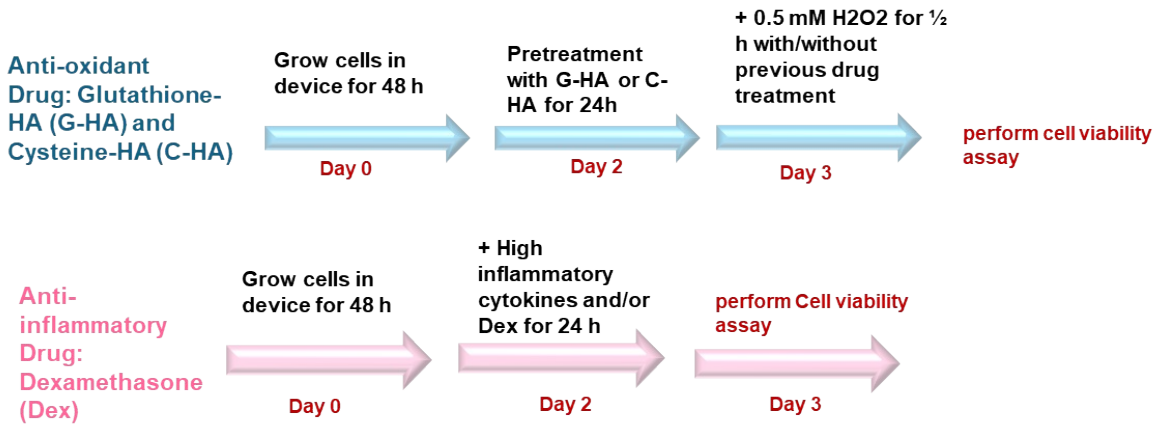


**Figure S13. Experimental design for ototoxic model development and drug effects analysis.**

Flow from MPS to Protein sensor

To facilitate fluid flow and analyte detection via GFET biosensor, it is necessary to couple the chip with a biocompatible microfluidic component. We have identified polydimethylsiloxane (PDMS) as a candidate material, based on methods previously described by Liu et al[3]. Given the small size of the GFET chip, as well as the material heterogeneity of the surface (silicon, graphene, gold), PDMS provides an acceptable balance of adhesiveness, biocompatibility, and castability[4]. Functioning chips exhibited an impedance value on the order of 1 kΩ, whereas destroyed sensors exhibited an impedance value on the order of 10 MΩ. This allows for quality control of the GFET chip to ensure that the graphene pads are still functional after attaching a microfluidic adaptor (**Figure S14A**).

Protein sensor measurement

We employed the integrated protein sensor to assess the sensor efficacy by measuring TNF-α expression. The sensor was used to monitor macrophage-mediated inflammation in the MPS rather than the previous high-inflammation blend, ensuring that no exogenous cytokines were introduced to avoid influencing the cytokine sensing process. To validate the accuracy of the sensor, we tested three conditions: 1) conditional media collected from THP-1 cells (monocyte cell line) stimulated with phorbol 12-myristate 13-acetate (PMA) for the generation of macrophages, 2) PMA plus lipopolysaccharide (LPS) for a proinflammatory condition, and 3) media from THP-1 cells alone. The media were applied into the MPS for 24 hours and were collected directly from the microfluidic device (**Figure S14A**), allowing for precise real-time detection of cytokine levels and accurate assessment of inflammatory responses. Our cytokine sensor data closely aligned with the results obtained from TNF-α ELISA (undetectable vs. 0.001, 2.5 vs. 6.78, and 19.5 vs. 11.8 ng/mL) (**Figure S14B**), demonstrating the accuracy and reliability of the sensor for measuring cytokine levels. This correlation validates the sensor's performance in real-time monitoring of cytokine concentrations, providing a rapid and efficient alternative to traditional ELISA methods while maintaining comparable sensitivity and specificity.

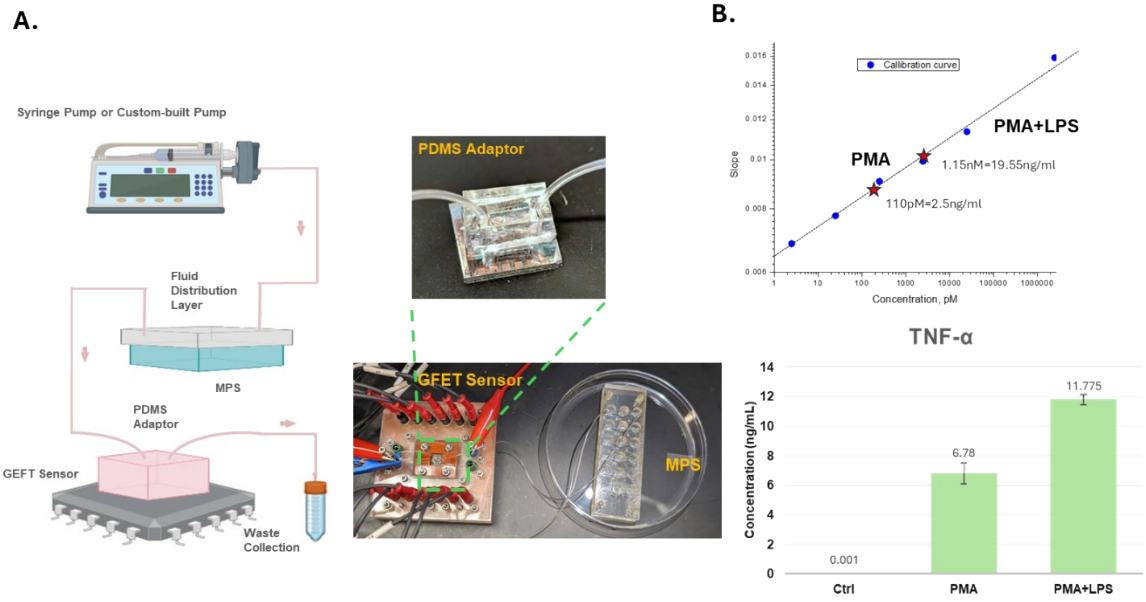

**Figure S14. The evaluation and validation of the integrated GFET sensor into MPS.** A. The layout of the integrated cytokine sensing platform. B. Analysis of TNF-α expression using the integrated sensor and compared with ELISA. Upper-GFET sensor results, lower-ELISA results. Ctrl- THP-1 conditional media without treatment.

## References


1. L. Xu, S. Ramadan, O. E. Akingbade, Y. Zhang, S. Alodan, N. Graham, K. A. Zimmerman, E. Torres, A. Heslegrave, P. K. Petrov, H. Zetterberg, D. J. Sharp, N. Klein and B. Li, *ACS Sens*, 2022, **7**, 253-262.
2. W. Y. Lai, J. W. Wang, B. T. Huang, E. P. Lin and P. C. Yang, *Theranostics*, 2019, **9**, 1741-1751.
3. H. Liu, O. A. Bolonduro, N. Hu, J. Ju, A. A. Rao, B. M. Duffy, Z. Huang, L. D. Black and B. P. Timko, *Nano Letters*, 2020, **20**, 2585-2593.
4. I. Miranda, A. Souza, P. Sousa, J. Ribeiro, E. M. S. Castanheira, R. Lima and G. Minas, *Journal of functional biomaterials*, 2021, **13**.